

Detecting relic gravitational waves in the CMB: Optimal parameters and their constraintsW. Zhao^{1,2,3,*} and D. Baskaran^{1,2,†}¹*School of Physics and Astronomy, Cardiff University, Cardiff, CF24 3AA, United Kingdom*²*Wales Institute of Mathematical and Computational Sciences, Swansea, SA2 8PP, United Kingdom*³*Department of Physics, Zhejiang University of Technology, Hangzhou, 310014, People's Republic of China*

(Received 10 February 2009; published 9 April 2009)

The prospect of detecting relic gravitational waves, through their imprint in the cosmic microwave background radiation, provides an excellent opportunity to study the very early Universe. In the simplest viable theoretical models the relic gravitational wave background is characterized by two parameters, the tensor-to-scalar ratio r and the tensor spectral index n_t . In this paper, we analyze the potential joint constraints on these two parameters, r and n_t , using the data from the upcoming cosmic microwave background radiation experiments. Introducing the notion of the best-pivot multipole ℓ_t^* , we find that at this pivot multipole the parameters r and n_t are uncorrelated, and have the smallest variances. We derive the analytical formulas for the best-pivot multipole number ℓ_t^* , and the variances of the parameters r and n_t . We verify these analytical calculations using numerical simulation methods, and find agreement to within 20%. The analytical results provide a simple way to estimate the detection ability for the relic gravitational waves by the future observations of the cosmic microwave background radiation.

DOI: [10.1103/PhysRevD.79.083003](https://doi.org/10.1103/PhysRevD.79.083003)

PACS numbers: 98.70.Vc, 04.30.-w, 98.80.Cq

I. INTRODUCTION

Detection of relic gravitational waves (RGWs) can be arguably considered one of the most important challenges for current and future cosmic microwave background radiation (CMB) experiments [1–5]. The RGWs are produced in the early Universe due to the superadiabatic amplification of zero point quantum fluctuations of the gravitational field [6]. For this reason, the RGWs carry invaluable information about the early history of our Universe that is inaccessible to any other medium (see review [7] for detailed discussion).

A whole range of scenarios of the early Universe, including the inflationary models, generically predict a RGW background with a power-law primordial power spectra [6,8–13]. In fact, the existence of RGWs is a consequence of quite general assumptions. Essentially, their existence relies only on the validity of general relativity and basic principles of quantum field theory [6]. The RGW backgrounds are conventionally characterized by two parameters, the so-called tensor-to-scalar ratio r and the primordial power spectral index of RGWs n_t (explained in detail below).

The RGWs leave well understood imprints on the anisotropies in temperature and polarization of CMB [14–19]. More specifically, RGWs produce a specific pattern of polarization in the CMB known as the B -mode polarization [15]. Moreover, RGWs produce a negative cross correlation between the temperature and polarization known as the TE correlation [18,20–22] (see also [23,24]). The theoretical analysis of these imprints along with the data

from CMB experiments allows one to place constraints on the parameters r and n_t describing the RGW background.

The current CMB experiments are yet to detect a definite signature of RGWs. It is hoped that, in the near future, with the launch of the Planck satellite [1] together with a host of ground-based [3] and balloon-borne [4] CMB experiments as well as the proposed satellite mission CMBPol [5], we shall be able to detect a definite signature of the RGW background. In light of this prospect, it is important to be able to effectively constrain the parameters r and n_t . A number of papers have discussed the current and potential constraint on the tensor-to-scalar ratio r [25]. However, most of these works either ignore the constraint on the spectral index n_t , or make simplifying assumptions about its value. One of the common simplifying assumptions is the so-called “consistency relation” $n_t = -r/8$ [26,27]. It should be noted that the consistency relation is valid only in the simplest models of inflation, namely, the single-field slow-roll inflationary model [26–28]. For a detailed critical discussion of inflationary predictions and data analysis based on these predictions see [29]. In order to keep our discussion sufficiently general we shall not use this consistency relation in our analysis.

The constraints on the parameters r and n_t , characterizing the RGW background, will give us a direct glimpse into the physical conditions in the early Universe. In particular, they will allow us to place a constraint on the Hubble parameter of the early Universe [30], which in the case of inflationary models would correspond to the constraints on the energy scale of inflation [26]. More specifically, the amplitude of the RGW power spectrum at a particular wavelength, characterized by r and n_t , determines the Hubble parameter at the time when the particular wavelength left the horizon. Thus, the determination of r and n_t

*Wen.Zhao@astro.cf.ac.uk

†Deepak.Baskaran@astro.cf.ac.uk

would give a direct measurement of the time evolution of the early Universe, and provide an observational tool to distinguish between the various inflationary-type models. In addition, the spectral index n_t has a special character if the RGW background is generated in a primordial Hagedorn phase of string cosmology [31] or inflation in the loop quantum gravity [32], so the determination of n_t provides an observational way to test or rule out these models.

In this paper we shall analyze the joint constraints on two parameters r and n_t that would be feasible with the analysis of the data from the upcoming CMB experiments. In general, there will be a nonvanishing correlation between parameters r and n_t [5,33]. As will be explained in the following sections, the definitions of r and n_t depend on a reference scale characterized by a multipole number ℓ_0 , which may be chosen arbitrarily. We shall show that with an appropriate choice of this multipole number, which we shall call the best multipole number ℓ_t^* (following the terminology of [34]), the parameters r and n_t become uncorrelated and have the smallest possible variances. We shall derive approximate analytical expressions for the variances and the correlation coefficients, followed by an analytical calculation of the pivot multipole ℓ_t^* . Using the Markov chain Monte Carlo (MCMC) simulation methods, we shall verify our analytical results and evaluate the expected constraints for realistic CMB experiments.

The outline of the paper is as follows. In Sec. II we shall introduce and explain the notations for the power spectra of gravitational waves, density perturbations and various CMB anisotropy fields and briefly explain how they are calculated. Furthermore, in this section we shall explicitly state the simplifying assumptions that we shall be using throughout the paper, and explain the limits of their applicability. Following this, in Sec. III, we shall calculate analytically the expected variances and the correlation associated with the parameters r and n_t . We shall show the existence of the best-pivot multipole scale ℓ_t^* for which the variances of the corresponding r and n_t are minimal and the correlation between them vanishes. In Sec. IV we shall confirm our analytical results using numerical calculations. Finally, Sec. V is dedicated to a brief discussion and conclusions.

II. POWER SPECTRA OF COSMOLOGICAL PERTURBATIONS AND CMB FIELDS

The main contribution to the observed temperature and polarization anisotropies of the CMB comes from two types of the cosmological perturbations, density perturbations (also known as the scalar perturbations) and RGWs (also known as the tensor perturbations) [10,11,14,15]. These perturbations are generally characterized by their primordial power spectra. These power spectra are usually assumed to be power laws, which is a generic prediction of a wide range of scenarios of the early Universe, including

the inflationary models. In general there might be deviations from a power law, which can be parametrized in terms of the running of the spectral index (see for example [27]), but we shall not consider this possibility in the current paper. Thus, the power spectra of the perturbation fields have the form

$$P_{\mathcal{R}}(k) = A_s(k_0) \left(\frac{k}{k_0} \right)^{n_s-1}, \quad (1)$$

$$P_h(k) = A_t(k_0) \left(\frac{k}{k_0} \right)^{n_t}, \quad (2)$$

for density perturbations and the RGWs, respectively. In the above expression k_0 is an arbitrarily chosen pivot wave number, n_s is the primordial power spectral index for density perturbations, and n_t is the primordial power spectral index for RGWs. $A_s(k_0)$ and $A_t(k_0)$ are normalization coefficients determining the absolute value of the primordial power spectra at the pivot wave number k_0 . The choices of $n_s = 1$ and $n_t = 0$ correspond to the scale-invariant power spectra for density perturbations and gravitational waves, respectively. The quantity $P_{\mathcal{R}}(k)$ is the primordial power spectrum of the curvature perturbation \mathcal{R} in the comoving gauge, i.e. $P_{\mathcal{R}}(k) = k^3 \langle |\mathcal{R}_k|^2 \rangle / 2\pi^2$ (see [35] for a detailed exposition). The quantity $P_h(k)$ is the primordial power spectrum of RGWs and gives the mean-square value of the gravitational field perturbations, in a logarithmic interval of the wave number k , at some initial epoch when the wavelengths of interest are well outside the horizon.

The relative contribution of density perturbations and gravitational waves is described by the so-called tensor-to-scalar ratio r defined as follows:

$$r(k_0) \equiv \frac{A_t(k_0)}{A_s(k_0)}. \quad (3)$$

Note that, in defining the tensor-to-scalar ratio r , we have not used any inflationary formulas which relate r with the physical conditions during inflation and the slow-roll parameters (see for example [26]). Thus, our definition depends only on the power spectral amplitudes of density perturbations and RGWs, and does not assume a particular generating mechanism for these cosmological perturbations.

Assuming that the amplitude of density perturbations $A_s(k_0)$ is known, taking into account the definitions (2) and (3), the power spectrum of the RGW field may be completely characterized by tensor-to-scalar ratio r and the spectral index n_t . The RGW amplitude $A_t(k_0) = r(k_0)A_s(k_0)$ provides us with direct information on the Hubble parameter of the very early Universe [30]. More specifically, this amplitude is directly related to the value of the Hubble parameter H at a time when wavelengths corresponding to the wave number k_0 crossed the horizon [6,8,9,30,36]

$$A_t^{1/2}(k_0) = \frac{\sqrt{2}}{M_{\text{pl}}} \frac{H}{\pi} \Big|_{k_0/a=H},$$

where $M_{\text{pl}} = 1/\sqrt{8\pi G}$ is the reduced Planck mass.

It is important to point out that, for spectral indices different from the invariant case (i.e. when $n_s \neq 1$ and $n_t \neq 0$), the definition of the tensor-to-scalar ratio depends on the pivot wave number k_0 . If we adopt different pivot wave number k_1 , the tensor-to-scalar ratio at this new pivot wave number $r(k_1)$ is related to original ratio $r(k_0)$ through the following relation [which follows from the definitions (1)–(3)]:

$$r(k_1) = r(k_0) \left(\frac{k_1}{k_0} \right)^{n_t - n_s + 1}. \quad (4)$$

Let us now turn our attention to CMB. Density perturbations and gravitational waves produce temperature and polarization anisotropies in the CMB characterized by the four angular power spectra C_ℓ^{TT} , C_ℓ^{EE} , C_ℓ^{BB} and C_ℓ^{TE} as functions of the multipole number ℓ . Here C_ℓ^{TT} is the power spectrum of the temperature anisotropies, C_ℓ^{EE} and C_ℓ^{BB} are the power spectra of the so-called E and B modes of polarization, respectively (note that density perturbation do not generate a B mode of polarization [15]), and C_ℓ^{TE} is the power spectrum of the temperature-polarization cross correlation. In what follows, we shall use the shorthand notations C_ℓ^T , C_ℓ^E , C_ℓ^B and C_ℓ^C to denote these spectra.

In general, the various power spectra C_ℓ^Y (where $Y = T, E, B$ or C) can be presented in the following form:

$$C_\ell^Y = C_{\ell,s}^Y + C_{\ell,t}^Y \quad (5)$$

where $C_{\ell,s}^Y$ is the power spectrum due to the density perturbations (scalar perturbations), and $C_{\ell,t}^Y$ is the power spectrum due to RGWs (tensor perturbations).

In the case of RGWs, the various CMB power spectra can be presented in the following form [16–18]:

$$\begin{aligned} C_{\ell,t}^Y &= (4\pi)^2 \int \frac{dk}{k} P_h(k) [\Delta_{Y\ell}^{(T)}(k)]^2, \quad \text{for } Y = T, E, B, \\ C_{\ell,t}^C &= (4\pi)^2 \int \frac{dk}{k} P_h(k) [\Delta_{T\ell}^{(T)}(k) \Delta_{E\ell}^{(T)}(k)]. \end{aligned} \quad (6)$$

Similar expressions hold in the case of CMB anisotropies due to density perturbations with a single exception. Density perturbations do not produce the B mode of polarization [15]. Thus, the CMB power spectra have the form [16]

$$\begin{aligned} C_{\ell,s}^Y &= (4\pi)^2 \int \frac{dk}{k} P_{\mathcal{R}}(k) [\Delta_{Y\ell}^{(S)}(k)]^2, \quad \text{for } Y = T, E, \\ C_{\ell,s}^C &= (4\pi)^2 \int \frac{dk}{k} P_{\mathcal{R}}(k) [\Delta_{T\ell}^{(S)}(k) \Delta_{E\ell}^{(S)}(k)]. \end{aligned} \quad (7)$$

The transfer functions $\Delta_{Y\ell}^{(S,T)}(k)$ (see [16–18] for details) in the above expressions translate the power in the metric

fluctuations (density perturbations or gravitational waves) into corresponding CMB power spectrum at an angular scale characterized by multipole ℓ . In general, these transfer functions are peaked at values $\ell \simeq (1.35 \times 10^4 \text{ Mpc}) \times k$, which is a reflection of the fact that metric fluctuations at a particular linear scale k^{-1} lead to CMB anisotropies predominantly at angular scales $\theta \sim kD$ (where D is the distance to the surface of last scattering). In this work, for numerical evaluation of the various CMB power spectra due to density perturbations and gravitational waves, we use the publicly available CAMB code [37].

Since we are primarily interested in the parameters of the RGW field, in the analytical and numerical analysis below we shall work with a fixed cosmological background model. More specifically, we shall work in the framework of Λ CDM model, and keep the background cosmological parameters fixed at the values determined by a typical model [38]

$$\begin{aligned} h &= 0.732, & \Omega_b h^2 &= 0.02229, & \Omega_m h^2 &= 0.1277, \\ \Omega_k &= 0, & \tau_{\text{reion}} &= 0.089. \end{aligned} \quad (8)$$

Furthermore, for density perturbations, we shall use a model with a primordial scalar perturbation power spectrum characterized by an amplitude and spectral index

$$A_s = 2.3 \times 10^{-9}, \quad n_s = 1.0. \quad (9)$$

In light of the above, CMB power spectra produced by RGWs depend on the tensor-to-scalar ratio r and the spectral index n_t . In general, this dependence is complicated and requires numerical calculations. For analytical calculations in Sec. III, we shall use a simple analytical approximation for this dependence (see for example [39])

$$C_{\ell,t}^Y \simeq \hat{C}_{\ell,t}^Y \left(\frac{r}{\hat{r}} \right) \left(\frac{\ell}{\ell_0} \right)^{n_t - \hat{n}_t} = \hat{C}_{\ell,t}^Y \left(\frac{r}{\hat{r}} \right) \exp[(n_t - \hat{n}_t) \ln(\ell/\ell_0)]. \quad (10)$$

Here $\hat{C}_{\ell,t}^Y = C_{\ell,t}^Y(r = \hat{r}, n_t = \hat{n}_t)$ are the spectra calculated for values of the tensor-to-scalar ratio and the spectral index fixed at fiducial values \hat{r} and \hat{n}_t , and ℓ_0 is the pivot multipole. The approximation (10) can be further simplified, for values of spectral index n_t sufficiently close to the fiducial value \hat{n}_t [such that $(n_t - \hat{n}_t) \ln(\ell/\ell_0) \ll 1$]:

$$C_{\ell,t}^Y \simeq \hat{C}_{\ell,t}^Y \left(\frac{r}{\hat{r}} \right) [1 + (n_t - \hat{n}_t) \ln(\ell/\ell_0)]. \quad (11)$$

The pivot multipole ℓ_0 is closely related to the pivot wave number k_0 . The approximation (10) can be derived from (2) and (6) under the assumption that the wave number k and multipole ℓ are linearly related, i.e. $k/k_0 \sim \ell/\ell_0$. This assumption is justified due to the peaked nature of transfer functions $\Delta_{Y,\ell}^{(T)}(k)$ entering (6). Numerical evaluations show that the pivot multipole is related to pivot wave number by

$$\ell_0 \approx k_0 \times 10^4 \text{ Mpc}. \quad (12)$$

For illustration, in Fig. 1 we plot the power spectra $C_{\ell,t}^Y$ for different values of the spectral index n_t . The pivot wave number is taken to be $k_0 = 0.05 \text{ Mpc}^{-1}$. As expected, in all the panels the spectra with different values of n_t converge at $\ell \simeq 500$, which is consistent with the prediction of the relation (12).

The CMB power spectra C_{ℓ}^Y are theoretical constructions determined by ensemble averages over all possible realizations of the underlying random process. However, in real CMB observations, we only have access to a single sky, and hence to a single realization. In order to obtain information on the power spectra from a single realization, it is required to construct estimators of power spectra. In order to differentiate the estimators from the actual power spectra, we shall use the notation D_{ℓ}^Y to denote the estimators while retaining the notation C_{ℓ}^Y to denote the power spectrum. It is important to keep in mind that the estimators D_{ℓ}^Y are constructed from observational data, while the power spectra C_{ℓ}^Y are theoretically predicted quantities. The probability density functions (pdfs) for the estimators are described in detail in the appendix. In what follows, we shall require the data from all the power spectral estima-

tors, i.e. D_{ℓ}^Y for $Y = T, E, B$, and C . Let us denote this set of estimators (which we shall sometimes refer to as the sample) as

$$\{D_{\ell}^Y\} \equiv \{D_{\ell}^Y | Y = C, T, E, B; \ell = 2, 3, \dots, \ell_{\max}\}.$$

To simulate an experiment, we shall randomly draw a data set $\{D_{\ell}^Y\}$ from the pdf (A1). In calculating the pdf (A1), along with parameters given in (8) and (9), we set the value of the RGW parameters as

$$r = \hat{r}, \quad n_t = \hat{n}_t. \quad (13)$$

We shall refer to \hat{r} and \hat{n}_t as the parameters of the input model.

For analytical evaluations in Sec. III, we shall work with Gaussian approximation to the exact pdfs (A1) for the estimators $\{D_{\ell}^Y\}$. The Gaussian approximation is characterized by corresponding mean values and standard deviations [22]

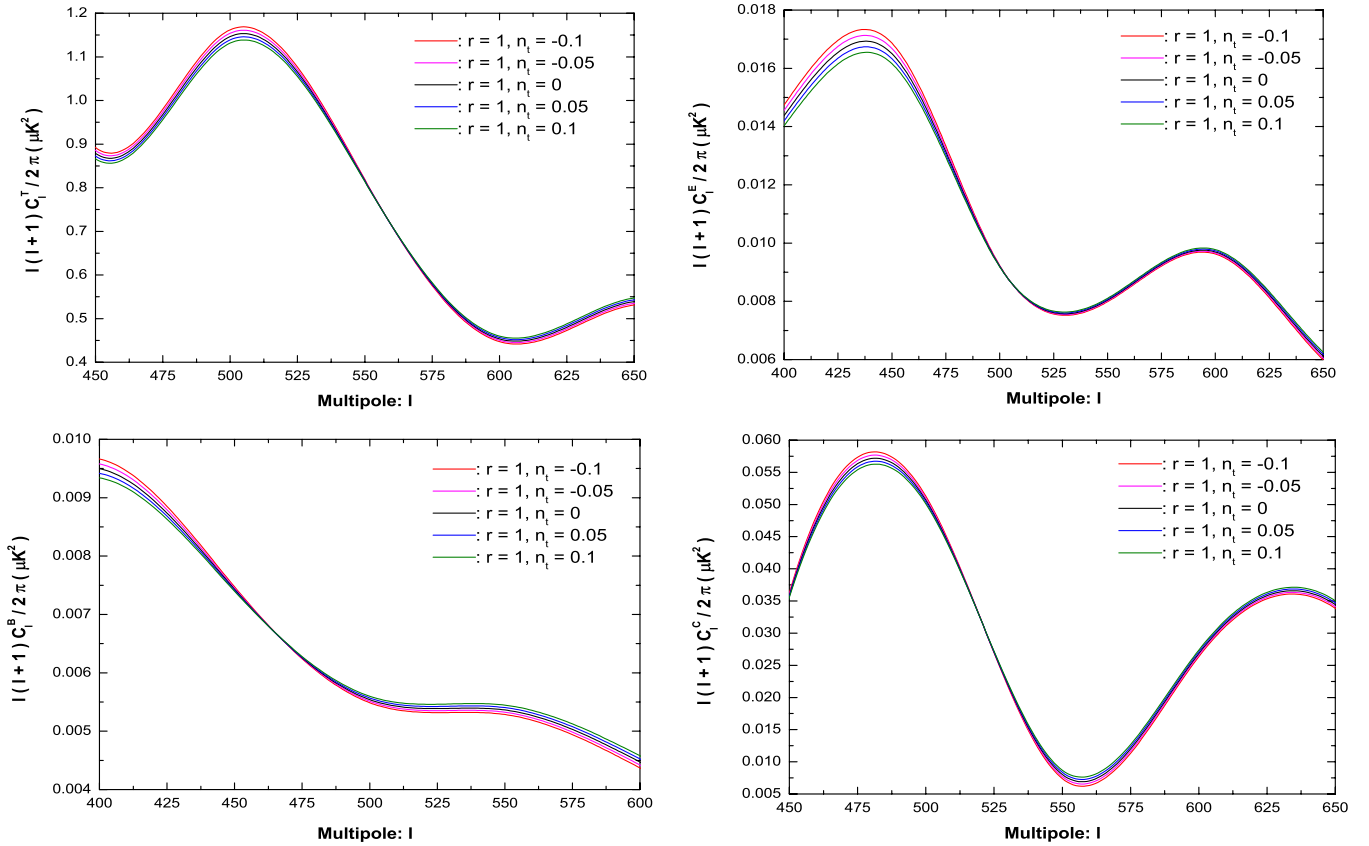


FIG. 1 (color online). The CMB power spectra due to RGWs for various values of the spectral index n_t : $C_{\ell,t}^T$ (left upper panel), $C_{\ell,t}^E$ (right upper panel), $C_{\ell,t}^B$ (left lower panel), $C_{\ell,t}^C$ (right lower panel). The pivot wave number is chosen $k_0 = 0.05 \text{ Mpc}^{-1}$ (in all the panels), and the power spectra are shown for multipoles around the value of the corresponding pivot multipole $\ell \sim 500$.

$$\begin{aligned}
 \langle D_\ell^Y \rangle &= C_\ell^Y, \quad (Y = T, E, B, C), \\
 \sigma_{D_\ell^Y} &= \sqrt{\frac{2}{(2\ell+1)f_{\text{sky}}}}(C_\ell^Y + N_\ell^Y W_\ell^{-2}) \quad (Y = T, E, B), \\
 \sigma_{D_\ell^C} &= \sqrt{\frac{(C_\ell^C)^2 + (C_\ell^T + N_\ell^T W_\ell^{-2})(C_\ell^E + N_\ell^E W_\ell^{-2})}{(2\ell+1)f_{\text{sky}}}}. \quad (14)
 \end{aligned}$$

Note that the above expressions for mean values and standard deviations follow from the exact pdfs considered in the appendix. In the above expression, N_ℓ^Y are the noise power spectra, f_{sky} is the cut sky factor, and W_ℓ is the window function.

In the case of the Planck mission [1], considering the channel at 143 GHz (which has the lower foreground level and lowest noise power spectra) the noise power spectra, the cut sky factor and the window function are given by [1] (see [22,40] for further explanations)

$$\begin{aligned}
 N_\ell^T &= 1.53 \times 10^{-4} \mu\text{K}^2, \quad N_\ell^E = N_\ell^B = 5.58 \times 10^{-4} \mu\text{K}^2, \\
 f_{\text{sky}} &= 0.65, \quad W_\ell = \exp\left[-\frac{\ell(\ell+1)}{2} \frac{\theta_{\text{FWHM}}^2}{8 \ln 2}\right], \quad (15)
 \end{aligned}$$

where $\theta_{\text{FWHM}} = 7.1'$ is the full width at half maximum of the Gaussian beam.

In this paper, along with predictions for Planck, we shall consider an idealized situation with no instrumental noise, full sky coverage and an idealized window function $W_\ell = 1$. For this case, we shall assume that the only source of noise comes from the contribution of cosmic lensing to the B mode of polarization. In this case the noise spectrum for the B mode is close to white with a value $N_\ell^B \simeq 2 \times 10^{-6} \mu\text{K}^2$ [41,42]. A number of works have discussed methods to subtract the lensing B -mode signal (see for example [41,43]). In [43], the authors claimed that a reduction in lensing power by a factor of 40 is possible using an approximate iterative maximum-likelihood method. For this reason, as a further idealized but feasible scenario, we shall also consider the case with reduced cosmic lensing noise $N_\ell^B \simeq 5 \times 10^{-8} \mu\text{K}^2$. Thus in the two described examples the noises are

$$\begin{aligned}
 N_\ell^B(\text{lensing}) &= 2 \times 10^{-6} \mu\text{K}^2, \\
 N_\ell^B(\text{reduced lensing}) &= 5 \times 10^{-8} \mu\text{K}^2; \quad (16) \\
 N_\ell^T &= N_\ell^E = 0; \quad f_{\text{sky}} = 1; \quad W_\ell = 1.
 \end{aligned}$$

Note that, in addition to the instrumental noises and lensing noise, various foregrounds, such as the synchrotron and dust, significantly contaminate the CMB signal. However, it is hoped that, using multifrequency observations together with ingenious foreground subtraction techniques, future experiments would be able to approach the ideal limit of expression (16) (see for instance [44]).

Before proceeding, let us briefly mention the notational conventions used in this paper. The *star* superscript denotes

the quantities evaluated at the best-pivot multipole ℓ_i^* . The *hat* superscript indicates the parameters of the fixed (input) cosmological model, that are used to generate the simulated observational data. The summation (product) symbols with subscript ℓ or Y indicate summation (product) for $\ell = 2, \dots, \ell_{\text{max}}$ and $Y = C, T, E, B$, respectively. In numerical evaluation we set $\ell_{\text{max}} = 1000$.

III. ANALYTICAL APPROXIMATION

In this section, we shall derive analytical expressions for the estimation of the parameters r and n_t , the associated uncertainties Δr and Δn_t and the correlation between these parameters. We will show the existence and explain the significance of the best-pivot multipole ℓ_i^* . Introducing the tensor-to-scalar ratio r^* defined at the best-pivot multipole, we shall show that this parameter can be determined with the smallest possible uncertainty, and is not correlated with the spectral index n_t . Based on this analysis, we shall discuss the signal-to-noise ratio and detection possibilities for various CMB experiments.

A. Approximation for the likelihood function

In order to estimate the parameters r and n_t characterizing the RGW background, we shall use an analysis based on the likelihood function [45,46]. The likelihood function is just the probability density function of the observational data considered as a function of the unknown parameters (which are r and n_t in our case). Up to a constant, independent of its arguments, the likelihood function is given by

$$\mathcal{L} = \prod_\ell f(D_\ell^C, D_\ell^T, D_\ell^E, D_\ell^B),$$

where the function $f(D_\ell^C, D_\ell^T, D_\ell^E, D_\ell^B)$ is explained in detail in the appendix.

For analysis in this section, we shall use a Gaussian function to approximate the pdf of the individual estimator D_ℓ^Y , and ignore any possible correlation between different estimators. In this case the approximate likelihood function can be written as (see [40] for details)

$$-2 \ln \mathcal{L} = \sum_\ell \sum_Y \left(\frac{D_\ell^Y - C_\ell^Y}{\sigma_{D_\ell^Y}} \right)^2. \quad (17)$$

The parameters r and n_t enter the above expression through the quantities C_ℓ^Y and $\sigma_{D_\ell^Y}$. In our analytical considerations we shall make a further simplification. We shall assume that $\sigma_{D_\ell^Y}$ entering (17) is weakly dependent on parameters r and n_t and assume $\sigma_{D_\ell^Y} = \hat{\sigma}_{D_\ell^Y}$ (for a justification of this assumption see [22,40]). With this assumption, the likelihood function can be rewritten as follows:

$$-2 \ln \mathcal{L} = \sum_\ell \sum_Y \left(\frac{D_\ell^Y - C_\ell^Y}{\hat{\sigma}_{D_\ell^Y}} \right)^2. \quad (18)$$

In the likelihood analysis, we shall assume that the value of the sought parameter n_t is sufficiently close to the input value \hat{n}_t . In this case, inserting (11) into (18), using (5), we can rewrite the likelihood in the form

$$-2 \ln \mathcal{L} = \sum_{\ell} \sum_Y \left\{ a_{\ell}^Y \left[\left(\frac{r}{\hat{r}} \right) (1 + (n_t - \hat{n}_t) b_{\ell}) \right] - d_{\ell}^Y \right\}^2, \quad (19)$$

where

$$a_{\ell}^Y \equiv \frac{\hat{C}_{\ell,t}^Y}{\hat{\sigma}_{D_{\ell}^Y}}, \quad b_{\ell} \equiv \ln \left(\frac{\ell}{\ell_0} \right), \quad d_{\ell}^Y \equiv \frac{D_{\ell}^Y - C_{\ell,t}^Y}{\hat{\sigma}_{D_{\ell}^Y}}. \quad (20)$$

Note that, in the above expression, the dependence on the data (on the estimators D_{ℓ}^Y) is solely contained in the term d_{ℓ}^Y . Furthermore, a_{ℓ}^Y , b_{ℓ} and d_{ℓ}^Y are independent of the RGW parameters r and n_t . The dependence on r and n_t takes a particularly simple form and is contained within the square brackets on the right side in (19).

In order to proceed, it is convenient to introduce new variables

$$\xi \equiv r/\hat{r}\zeta \equiv (n_t - \hat{n}_t)(r/\hat{r}), \quad (21)$$

in place of r and n_t . In terms of these variables, the likelihood (19) can be simplified as

$$-2 \ln \mathcal{L} = \sum_{\ell} \sum_Y [a_{\ell}^Y (\xi + \zeta b_{\ell}) - d_{\ell}^Y]^2. \quad (22)$$

Note that the dependence on the sought for parameters r and n_t , in the above expression, is contained in the variables ξ and ζ . After straightforward manipulations (22) can be rewritten as

$$\begin{aligned} -2 \ln \mathcal{L} &= \xi^2 \left(\sum_{\ell} \sum_Y a_{\ell}^{Y2} \right) + \zeta^2 \left(\sum_{\ell} \sum_Y (a_{\ell}^Y b_{\ell})^2 \right) \\ &+ 2\xi\zeta \left(\sum_{\ell} \sum_Y a_{\ell}^{Y2} b_{\ell} \right) - 2\xi \left(\sum_{\ell} \sum_Y a_{\ell}^Y d_{\ell}^Y \right) \\ &- 2\zeta \left(\sum_{\ell} \sum_Y a_{\ell}^Y d_{\ell}^Y b_{\ell} \right) + \sum_{\ell} \sum_Y d_{\ell}^{Y2}. \end{aligned}$$

This expression can be rewritten as

$$\begin{aligned} -2 \ln \mathcal{L} &= \left(\sum_{\ell} \sum_Y a_{\ell}^{Y2} \right) \left(\xi - \frac{\sum_{\ell} \sum_Y a_{\ell}^Y d_{\ell}^Y}{\sum_{\ell} \sum_Y a_{\ell}^{Y2}} \right)^2 \\ &+ \left(\sum_{\ell} \sum_Y (a_{\ell}^Y b_{\ell})^2 \right) \left(\zeta - \frac{\sum_{\ell} \sum_Y a_{\ell}^Y b_{\ell} d_{\ell}^Y}{\sum_{\ell} \sum_Y (a_{\ell}^Y b_{\ell})^2} \right)^2 \\ &+ 2\xi\zeta \left(\sum_{\ell} \sum_Y a_{\ell}^{Y2} b_{\ell} \right) + C, \quad (23) \end{aligned}$$

where C is a constant, independent of r and n_t . This

constant is responsible for the overall normalization of the likelihood function and will not participate in estimation of parameters. In the following subsection we shall use the approximation (23) for estimating the parameters r and n_t .

B. Posterior pdf and the best-pivot multipole ℓ_t^*

1. Posterior pdf

The constraints on the parameters r and n_t are determined by the posterior probability density function $P(r, n_t)$. This posterior pdf is related to the likelihood function \mathcal{L} by [45,46]

$$P(r, n_t) = f(r, n_t) \mathcal{L}, \quad (24)$$

where $f(r, n_t)$ is the prior probability density function of the parameters r and n_t . In this paper, we adopt a flat prior, i.e.

$$f(r, n_t) = 1. \quad (25)$$

Thus, in this case, the posterior pdf $P(r, n_t)$ becomes equal to the likelihood. Using the approximation (23) for the likelihood, we obtain

$$\begin{aligned} -2 \ln P(r, n_t) &= \left(\sum_{\ell} \sum_Y a_{\ell}^{Y2} \right) \left(\xi - \frac{\sum_{\ell} \sum_Y a_{\ell}^Y d_{\ell}^Y}{\sum_{\ell} \sum_Y a_{\ell}^{Y2}} \right)^2 \\ &+ \left(\sum_{\ell} \sum_Y (a_{\ell}^Y b_{\ell})^2 \right) \left(\zeta - \frac{\sum_{\ell} \sum_Y a_{\ell}^Y b_{\ell} d_{\ell}^Y}{\sum_{\ell} \sum_Y (a_{\ell}^Y b_{\ell})^2} \right)^2 \\ &+ 2\xi\zeta \left(\sum_{\ell} \sum_Y a_{\ell}^{Y2} b_{\ell} \right) + C. \quad (26) \end{aligned}$$

The parameters r and n_t enter the above expression through the variables ξ and ζ . For this reason it is convenient to first consider the posterior pdf for variables ξ and ζ . It will be seen that the posterior pdf for these variables will have a particularly simple form, namely, a bivariate normal function. The posterior pdf $P(\xi, \zeta)$ is related to $P(r, n_t)$ in the following manner:

$$P(\xi, \zeta) = \left| \frac{\partial(r, n_t)}{\partial(\xi, \zeta)} \right| P(r, n_t) = \frac{\hat{r}}{\xi} P(r, n_t), \quad (27)$$

where $\left| \frac{\partial(r, n_t)}{\partial(\xi, \zeta)} \right|$ denotes the Jacobian of the transformation between the two sets of variables calculable from (21). For simplicity and clarity, let us first consider the constraints on the parameters ξ and ζ . Following this, we shall return to the discussion on r and n_t using relation (27).

Introducing the notations

$$\begin{aligned}\xi_p &\equiv \left(\sum_{\ell} \sum_Y a_{\ell}^Y d_{\ell}^Y \right) / \left(\sum_{\ell} \sum_Y a_{\ell}^{Y2} \right), \\ \xi_s &\equiv 1 / \sqrt{\sum_{\ell} \sum_Y a_{\ell}^{Y2}}, \\ \zeta_p &\equiv \left(\sum_{\ell} \sum_Y a_{\ell}^Y d_{\ell}^Y b_{\ell} \right) / \left(\sum_{\ell} \sum_Y (a_{\ell}^Y b_{\ell})^2 \right), \\ \zeta_s &\equiv 1 / \sqrt{\sum_{\ell} \sum_Y (a_{\ell}^Y b_{\ell})^2},\end{aligned}\quad (28)$$

from (26) and (27), we obtain that expression for the posterior pdf of ξ and ζ in the form

$$\begin{aligned}P(\xi, \zeta) &= \frac{\hat{r}e^C}{\xi} \exp\left[-\frac{(\xi - \xi_p)^2}{2(\xi_s)^2}\right] \exp\left[-\frac{(\zeta - \zeta_p)^2}{2(\zeta_s)^2}\right] \\ &\times \exp\left[-\xi\zeta\left(\sum_{\ell} \sum_Y a_{\ell}^{Y2} b_{\ell}\right)\right].\end{aligned}\quad (29)$$

2. Best-pivot multipole ℓ_t^*

Let us concentrate on the posterior pdf (29). As can be seen, there is a nonvanishing correlation between the parameters ξ and ζ in the case when $\sum_{\ell} \sum_Y a_{\ell}^{Y2} b_{\ell} \neq 0$. From the definition (20), it follows that the terms b_{ℓ} depend on the arbitrarily chosen pivot multipole ℓ_0 [corresponding to the pivot wave number k_0 through the relation (12)]. For this reason, we can select the pivot multipole $\ell_0 = \ell_t^*$ so as to require

$$\sum_{\ell} \sum_Y a_{\ell}^{Y2} b_{\ell}^* = 0, \quad (30)$$

where $b_{\ell}^* \equiv b_{\ell}|_{\ell_0=\ell_t^*}$. With this choice of pivot multipole ℓ_t^* , and the corresponding pivot wave number k_t^* , the variables $\xi(k_t^*)$ and $\zeta(k_t^*)$ will have no correlation. We shall refer to this pivot multipole ℓ_t^* as the best-pivot multipole number. From definitions (20) of a_{ℓ}^Y and b_{ℓ} , along with expression (14), it follows that the precise numerical value of the best-pivot multipole number ℓ_t^* depends on the input cosmological model characterized by (8), (9), and (13), as well as the specifics of the CMB experiment characterized by noise power spectra, cut sky factor and window function. We shall discuss this dependence in more detail below.

Setting the value of the pivot multipole $\ell_0 = \ell_t^*$, so as to satisfy (30), we arrive at a simplified form for the posterior pdf:

$$\begin{aligned}P(\xi^*, \zeta^*) &= (\hat{r}e^C) \frac{1}{\xi^*} \exp\left[-\frac{(\xi^* - \xi_p^*)^2}{2(\xi_s^*)^2}\right] \\ &\times \exp\left[-\frac{(\zeta^* - \zeta_p^*)^2}{2(\zeta_s^*)^2}\right].\end{aligned}\quad (31)$$

As a reminder let us point out that, in the above expression, as well as in what follows, we have used notations r^* , ξ^* , ζ^* and b_{ℓ}^* to denote the corresponding quantities calculated for the pivot multipole chosen at the best-pivot multipole value ℓ_t^* . Note that for the spectral index of RGWs we shall retain the notation n_t , since it does not depend on the choice of the pivot multipole.

3. Constraints on parameters ξ^* and ζ^*

Equipped with the posterior pdf (31), let us analyze the uncertainties in determining the parameters ξ^* and ζ^* . For simplicity of analysis we shall assume

$$\xi_p^* \gg \xi_s^*. \quad (32)$$

In Sec. III F, we shall show that this constraint corresponds to a condition that the signal-to-noise ratio is large, i.e. $S/N \gg 1$. Taking into account this condition, the posterior function (31) may be further approximated in the following manner:

$$P(\xi^*, \zeta^*) \simeq \frac{\hat{r}e^C}{\xi_p^*} \exp\left[-\frac{(\xi^* - \xi_p^*)^2}{2(\xi_s^*)^2}\right] \exp\left[-\frac{(\zeta^* - \zeta_p^*)^2}{2(\zeta_s^*)^2}\right]. \quad (33)$$

Note that, in the above expression, the factor in front of the exponent $\hat{r}e^C/\xi_p^*$ now becomes a constant independent of ξ^* and ζ^* . Thus, the posterior pdf $P(\xi^*, \zeta^*)$ becomes a bivariate normal (Gaussian) function for variables ξ^* and ζ^* . The position of the maximum and the standard deviation associated with the posterior pdf $P(\xi^*, \zeta^*)$ are given by

$$\xi_{\text{ML}}^* = \xi_p^*, \quad \Delta \xi^* = \xi_s^*, \quad \zeta_{\text{ML}}^* = \zeta_p^*, \quad \Delta \zeta^* = \zeta_s^*. \quad (34)$$

In the above expression, subscript ‘‘ML’’ stands for ‘‘maximum-likelihood,’’ since the maximum of the posterior pdf coincides with that of the likelihood function due to (24) and (25). Following the maximum-likelihood parameters estimation procedure, we shall accept the values ξ_{ML}^* and ζ_{ML}^* as the estimators for the corresponding quantities ξ^* and ζ^* . It is worth mentioning that, for the posterior pdfs considered in this work, the maximum-likelihood values coincide with the mean values of the corresponding posterior pdfs. It is worth mentioning that the assumption $\xi_p^* \gg \xi_s^*$ [which was used to derive the pdf (33)] is equivalent to the requirement $\xi_{\text{ML}}^* \gg \Delta \xi^*$.

Proceeding further, we can calculate the correlation coefficient for variables ξ^* and ζ^* . Let us first define the covariance in the following manner:

$$\text{cov}(x, y) \equiv \overline{(x - \bar{x})(y - \bar{y})}, \quad (35)$$

where the overline indicates averaging over the corresponding posterior pdf. The correlation coefficient can now be explicitly calculated to give

$$\rho_{(\xi^*, \zeta^*)} \equiv \frac{\text{cov}(\xi^*, \zeta^*)}{\sqrt{\text{cov}(\xi^*, \xi^*)\text{cov}(\zeta^*, \zeta^*)}} = 0, \quad (36)$$

and as expected, the correlation between the variables ξ^* and ζ^* vanishes.

Taking into account (28), we find that the mean values $\bar{\xi}^*$ (also ξ_{ML}^*) and $\bar{\zeta}^*$ (also ζ_{ML}^*) depend on data $\{D_\ell^Y\}$ through quantities d_ℓ^Y . However, in our approximation, the standard deviations $\Delta\xi^*$ and $\Delta\zeta^*$ are independent of the data. They depend on the input cosmological model determined by (8), (9), and (13), along with noises, cut sky factor and the window function characterizing the CMB experiment.

C. Constraints on parameters r^* and n_t

Let us now return to the parameters of our direct interest, namely, the tensor-to-scalar ratio (determined at the best-pivot wave number) r^* and RGW primordial spectral index n_t . These parameters are related to ξ^* and ζ^* through relations

$$r^* = \hat{r}^* \xi^*, \quad n_t = \hat{n}_t + \zeta^*/\xi^*, \quad (37)$$

which follow from (21). Taking into account the fact that the quantity ξ^* is peaked at ξ_{ML}^* which is sufficiently close to the input value $\hat{\xi}^*$, and $\Delta\xi^*/\xi_{\text{ML}}^* \ll 1$, we can approximate the quantity ξ^* in the expression for n_t [see the second formula in (37)] with 1. Thus (37) can be written as

$$r^* = \hat{r}^* \xi^*, \quad n_t \simeq \hat{n}_t + \zeta^*. \quad (38)$$

Using (27), the posterior pdf for r^* and n_t is related to $P(\xi^*, \zeta^*)$ in the following way:

$$P(r^*, n_t) = \frac{\xi^*}{\hat{r}^*} P(\xi^*, \zeta^*) \simeq \frac{\xi^*}{\hat{r}^*} P(\xi^*, \zeta^*). \quad (39)$$

Note that, in the current approximation, the pdf for variables r^* and n_t has a bivariate normal form.

Based on the above pdf (39), we can now evaluate the maximum-likelihood estimators, standard deviations, and the correlation coefficient for the variables r^* and n_t . For the maximum-likelihood values we get

$$r_{\text{ML}}^* = \hat{r}^* \xi_{\text{ML}}^* = \hat{r}^* \frac{\sum_\ell \sum_Y a_\ell^Y d_\ell^Y}{\sum_\ell \sum_Y a_\ell^{Y2}}, \quad (40)$$

$$n_{t\text{ML}} \simeq \hat{n}_t + \zeta_{\text{ML}}^* = \hat{n}_t + \frac{\sum_\ell \sum_Y a_\ell^Y d_\ell^Y b_\ell^*}{\sum_\ell \sum_Y (a_\ell^Y b_\ell^*)^2}.$$

The standard deviations are given by

$$\Delta r^* = \hat{r}^* \Delta\xi^* = \hat{r}^* / \sqrt{\sum_\ell \sum_Y a_\ell^{Y2}}, \quad (41)$$

$$\Delta n_t \simeq \Delta\zeta^* = 1 / \sqrt{\sum_\ell \sum_Y (a_\ell^Y b_\ell^*)^2}.$$

Finally, it can be shown that the correlation between r^* and n_t vanishes:

$$\rho_{(r^*, n_t)} \equiv \frac{\text{cov}(r^*, n_t)}{\sqrt{\text{cov}(r^*, r^*)\text{cov}(n_t, n_t)}} = 0. \quad (42)$$

It is interesting to point out that these results are consistent with the results in [40]. The constraints, presented in this paper, on the tensor-to-scalar ratio r are exactly the same as those in [40]. Unlike the analysis in the current paper, [40] works with a single free parameter r and does not consider n_t as an independent free parameter.

D. Constraints on parameter r

In Sec. III C, using the posterior probability function $P(r^*, n_t)$, we have investigated the tensor-to-scalar ratio r^* and the spectral index n_t defined at the best-pivot wave number k_t^* (corresponding to the best-pivot multipole ℓ_t^*). We can now proceed to the analysis of the tensor-to-scalar ratio r , defined at an arbitrary pivot wave number k_0 , and determine the possible constraints on this parameter.

From Eq. (4), we can express the tensor-to-scalar ratio r , in terms of r^* , k_t^* and the spectral indices n_t and n_s , in the following form:

$$\ln r = \ln r^* + n_t \ln(k_0/k_t^*) + (1 - n_s) \ln(k_0/k_t^*). \quad (43)$$

It can be seen that, for a fixed value of the spectral index n_s [see (9)], r depends on the parameters r^* and n_t . Thus, the properties of r can be determined using the posterior pdf $P(r^*, n_t)$, which was analyzed in detail in Sec. III C. In the case $k_0 \neq k_t^*$ it is more illustrative to consider the variable $\ln r$ instead of the variable r . For this reason, when dealing with the maximum-likelihood estimators of the tensor-to-scalar ratio defined at a pivot scale different from the best-pivot scale, we shall use the corresponding logarithms

$$\ln r_{\text{ML}} = \ln r_{\text{ML}}^* + n_{t\text{ML}} \ln(k_0/k_t^*) + (1 - n_s) \ln(k_0/k_t^*), \quad (44)$$

where r_{ML}^* and $n_{t\text{ML}}$ are the maximum-likelihood estimators expressible in terms of the input parameters \hat{r}^* , \hat{n}_t and the data $\{D_\ell^X\}$ [see (40)]. The uncertainty of r can be expressed in terms of the uncertainties Δr^* and Δn_t determined in (41), leading to the following expression:

$$\Delta \ln r \simeq \sqrt{(\Delta r^*/\hat{r}^*)^2 + (\ln(k_0/k_t^*)\Delta n_t)^2} \\ = \sqrt{(\xi_s^*)^2 + (\ln(k_0/k_t^*)\zeta_s^*)^2}. \quad (45)$$

The quantities ξ_s^* and ζ_s^* , entering the above expression, can be expressed through CMB power spectra due to RGWs $C_{\ell,t}^X$ using (20) and (28).

From (45) it follows that $\Delta r/r \geq \Delta r^*/r^*$, with the equality holding for $k_0 \rightarrow k_t^*$. Thus, the smallest uncertainty on tensor-to-scalar ratio r is achieved for the choice of the pivot scale $k_0 = k_t^*$. This justifies the title ‘‘best’’-pivot wave number for k_t^* . For a choice of pivot wave

number $k_0 \neq k_t^*$ the uncertainty in determining r becomes larger due to the uncertainty in determining the spectral index n_t .

Although, as was shown in Sec. III C, the quantities r^* and n_t are uncorrelated, this is not true for the quantities r and n_t in general. In order to describe the correlation between r and n_t , it is convenient to introduce the correlation coefficient

$$\rho_{(n_t, \ln r)} \equiv \frac{\text{cov}(n_t, \ln r)}{\sqrt{\text{cov}(n_t, n_t) \text{cov}(\ln r, \ln r)}}, \quad (46)$$

where the notation $\text{cov}(\cdot, \cdot)$ for the covariance was defined in (35). Using this definition, along with (42) and (43), the terms entering the above expression can be evaluated as

$$\begin{aligned} \text{cov}(\ln r, \ln r) &= (\Delta \ln r)^2, & \text{cov}(n_t, n_t) &= (\Delta n_t)^2, \\ \text{cov}(n_t, \ln r) &= \text{cov}(n_t, \ln r^*) + (\ln(k_0/k_t^*)) \text{cov}(n_t, n_t) \\ &= (\ln(k_0/k_t^*)) (\Delta n_t)^2. \end{aligned}$$

Taking into account (41), the correlation coefficient can be presented in the following form:

$$\rho_{(n_t, \ln r)} = \sqrt{\frac{\zeta_s^{*2} (\ln(k_0/k_t^*))^2}{\zeta_s^{*2} (\ln(k_0/k_t^*))^2 + \xi_s^{*2}}}. \quad (47)$$

As expected, for choice the $k_0 = k_t^*$, i.e. when the pivot wave number is chosen at the value of the best-pivot wave number, the correlation between r and n_t vanishes. On the other hand, for $|\ln(k_0/k_t^*)| \gg 1$, i.e. for values of the pivot wave number significantly different from the best-pivot wave number, the correlation coefficient approaches unity, implying a strong correlation between r and n_t .

E. Statistical properties of maximum-likelihood estimators

The exact numerical values of the maximum-likelihood (ML) estimators ξ_{ML}^* , ζ_{ML}^* , r_{ML}^* , $n_{t\text{ML}}$ and $\ln r_{\text{ML}}$ discussed in the previous subsections depend on the CMB data $\{D_\ell^Y\}$. Since the set $\{D_\ell^Y\}$ is a single realization of an underlying random process characterized by the pdf (A1), the precise values of the maximum-likelihood estimators will depend on this realization. For this reason, it is instructive to analyze the distribution of these maximum-likelihood estimators in various realizations of the underlying random process specified by the pdf for estimators of the CMB power spectrum $\{D_\ell^X\}$. Heuristically speaking, the mean value of this distribution characterizes the typical value for the ML estimators that we are likely to observe (for a specific input cosmological model), while the standard deviation characterizes the typical departure from the mean value.

Let us first, for simplicity, consider the estimators ξ_{ML}^* and ζ_{ML}^* . The expectation values for these estimators can be calculated in the following manner:

$$\begin{aligned} \langle \xi_{\text{ML}}^* \rangle &= \left\langle \left(\frac{\sum_\ell \sum_Y a_\ell^Y d_\ell^Y}{\sum_\ell \sum_Y a_\ell^{Y2}} \right) \right\rangle \\ &= \left(\frac{\sum_\ell \sum_Y a_\ell^Y \langle d_\ell^Y \rangle}{\sum_\ell \sum_Y a_\ell^{Y2}} \right) = 1, \\ \langle \zeta_{\text{ML}}^* \rangle &= \left\langle \left(\frac{\sum_\ell \sum_Y a_\ell^Y d_\ell^Y b_\ell^*}{\sum_\ell \sum_Y (a_\ell^Y b_\ell^*)^2} \right) \right\rangle \\ &= \left(\frac{\sum_\ell \sum_Y a_\ell^Y \langle d_\ell^Y \rangle b_\ell^*}{\sum_\ell \sum_Y (a_\ell^Y b_\ell^*)^2} \right) = 0. \end{aligned} \quad (48)$$

The angle brackets $\langle \dots \rangle$, in the above expression and elsewhere in the text, denote the ensemble average over the joint pdf (A1). Furthermore, in this pdf, the input values for the tensor-to-scalar ratio and spectral index are chosen as $r = \hat{r}$ and $n_t = \hat{n}_t$, respectively. In deriving the above expressions we have first used (28) and (34). We have also used the identity $\langle d_\ell^X \rangle = a_\ell^X$ which follows directly from (5), (14), and (20). Finally, in the bottom line, we have used the definition of the best-pivot multipole (30). Similarly, the standard deviations can be calculated to yield

$$\sigma_{\xi_{\text{ML}}^*} = \xi_s^*, \quad \sigma_{\zeta_{\text{ML}}^*} = \zeta_s^*. \quad (49)$$

Proceeding in an identical manner, the expectation values and standard deviations for the maximum-likelihood estimators r_{ML}^* , $n_{t\text{ML}}$ and $\ln r_{\text{ML}}$ are given by

$$\begin{aligned} \langle r_{\text{ML}}^* \rangle &= \hat{r}^* \langle \xi_{\text{ML}}^* \rangle = \hat{r}^*, & \langle n_{t\text{ML}} \rangle &= \hat{n}_t + \langle \zeta_{\text{ML}}^* \rangle = \hat{n}_t, \\ \langle \ln r_{\text{ML}} \rangle &= \ln \hat{r}^* + (\hat{n}_t - n_s + 1) \ln(k_0/k_t^*) = \ln \hat{r}, \end{aligned} \quad (50)$$

and

$$\begin{aligned} \sigma_{r_{\text{ML}}^*} &= \hat{r}^* \sigma_{\xi_{\text{ML}}^*} = \hat{r}^* \xi_s^*, & \sigma_{n_{t\text{ML}}} &= \sigma_{\zeta_{\text{ML}}^*} = \zeta_s^*, \\ \sigma_{\ln r_{\text{ML}}} &\simeq \sqrt{(\xi_s^*)^2 + (\ln(k_0/k_t^*) \zeta_s^*)^2}. \end{aligned} \quad (51)$$

As expected, from expression (50) it can be seen that the constructed ML estimators are unbiased. Furthermore, the standard deviation of the estimator $\sigma_{\ln r_{\text{ML}}}$ strongly depends on the choice of the pivot multipole k_0 , and is minimal for the choice $k_0 = k_t^*$. We shall numerically verify these results in the following section.

F. The dependence of results on cosmological parameters and experimental noises

Let us now address the question of detection of RGWs in various CMB experiments. In order to quantify the ability to detect the signature of RGWs in the CMB data, it is convenient to define the signal-to-noise ratio as follows [22,40]:

$$S/N \equiv \frac{\hat{r}^*}{\Delta r^*}. \quad (52)$$

Using expression (41) we arrive at an elegant expression for the signal-to-noise ratio:

$$S/N = \sqrt{\sum_{\ell} \sum_Y \left(\frac{\hat{C}_{\ell,t}^Y}{\hat{\sigma}_{D_t^Y}} \right)^2}. \quad (53)$$

Thus, the signal-to-noise ratio contains contributions from individual power spectra and individual multipoles. These contributions have a clear physical meaning. For a particular power spectrum and a particular multipole, they represent the ratio of the expected signal due to RGWs to the overall uncertainty.

As was mentioned in Sec. III B, for the analytical estimations, we had assumed $\xi_p^* \gg \xi_s^*$ [see (32)]. We can now relate this condition to the requirement on the value of the signal-to-noise ratio S/N . Using Eqs. (34), (40), and (41), we find that

$$\frac{\xi_p^*}{\xi_s^*} = \frac{r_{\text{ML}}^*}{\Delta r^*} \simeq \frac{\hat{r}^*}{\Delta r^*} = S/N. \quad (54)$$

Hence, the condition $\xi_p^* \gg \xi_s^*$ corresponds to the requirement $S/N \gg 1$, i.e. to the requirement that the RGW signal may be well determined at a high signal-to-noise ratio.

In the discussion above we have mentioned that the best-pivot multipole ℓ_t^* , the signal-to-noise ratio S/N and the uncertainty in determination of the RGW spectral index Δn_t depend on the input cosmological model and the specifics of the CMB experiment. Let us analyze this dependence in more detail.

The input cosmological model is determined by specifying the background cosmological model, along with the parameters determining the density perturbations and gravitational waves. The background cosmological pa-

rameters and contribution from density perturbations are fairly well constrained by the current observations [38]. The variation of these parameters within the margin allowed by these constraints will not significantly alter our results. For this reason, we shall fix the background cosmological model using the values of the typical Λ CDM model (8). We shall also fix the contribution of density perturbations at a value (9). Furthermore, numerical calculations show that the dependence of various parameters on the input value of the spectral index \hat{n}_t is weak, and for this reason in evaluations of this section we shall set $\hat{n}_t = 0$. Thus, we shall be interested in the dependence of the parameters on value of the input tensor-to-scalar ratio \hat{r} . Figure 2 shows the values of quantities ℓ_t^* , S/N and Δn_t as functions of \hat{r}^* , calculated using the expressions (30), (41), and (53).

As was explained in Sec. II, the specifics of the CMB experiment are determined by the noise power spectra, the cut sky factor and window function. In this section we shall consider the parameters ℓ_t^* , S/N and Δn_t for the three cases specified in Sec. II [see (15) and (16)]. The different curves (solid, dashed and dotted) on the three panels in Fig. 2 show the corresponding values of quantities ℓ_t^* , S/N and Δn_t for these three noise scenarios.

The left panel of Fig. 2 shows the best-pivot multipole ℓ_t^* as a function of the input tensor-to-scalar ratio \hat{r}^* which is defined with respect to the best-pivot multipole. It can be seen that, for small values of \hat{r}^* , the best-pivot multipole ℓ_t^* is small. This behavior can be easily understood. For small values of \hat{r}^* , the constraints on r^* and n_t mainly come from B -mode power spectrum [40]. However, in the B mode the main contribution to the signal comes from large angular

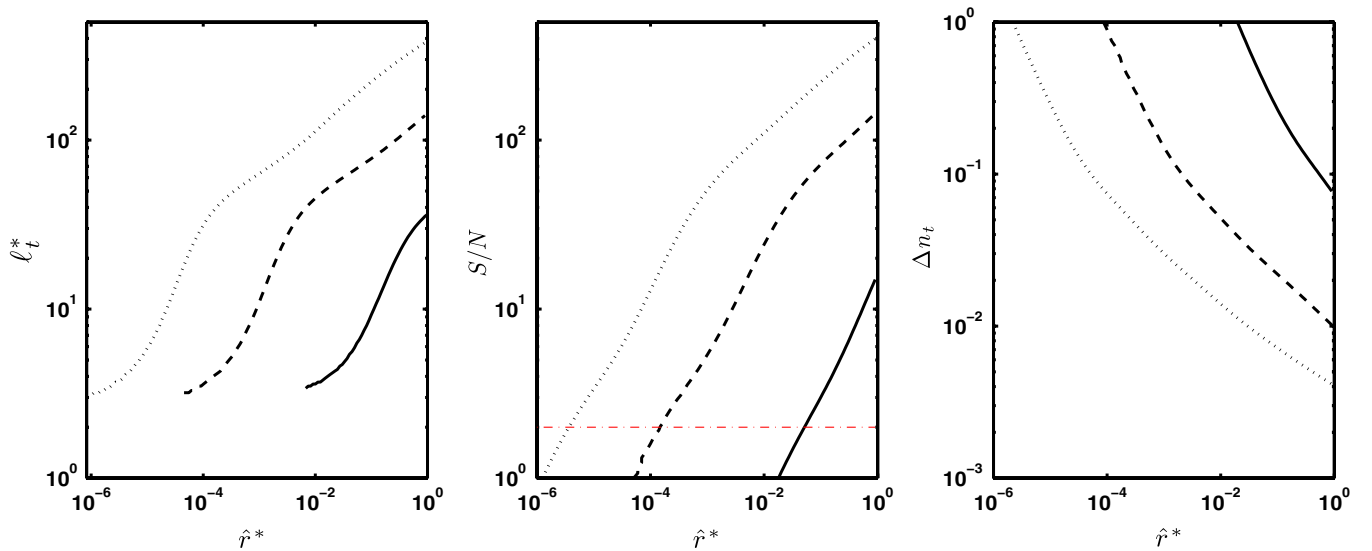


FIG. 2 (color online). The figures show the value of the best-pivot multipole ℓ_t^* (left panel), signal-to-noise ratio S/N (middle panel) and the uncertainty in the RGW spectral index Δn_t (right panel) as functions of the tensor-to-scalar ratio \hat{r}^* . The solid lines correspond to the Planck instrumental noises [see (15)]; the dashed lines correspond to noises from cosmic lensing [see (16)]; the dotted lines correspond to reduced cosmic lensing noise [see (16)].

scales corresponding to $\ell \lesssim 10$, where the signal is mainly due to cosmic reionization [22,40]. Thus, for small \hat{r}^* , the constraints on parameters r and n_t are most stringently determined at large angular scales corresponding to multipoles $\ell \lesssim 10$. For this reason, for small values of \hat{r}^* the best-pivot multipole is small, corresponding to the scale at which the parameters r and n_t are most stringently determined. On the other hand, for large values \hat{r}^* , the best-pivot multipole ℓ_t^* also becomes large. This happens due to two reasons. First, with an increase in value of \hat{r}^* , the relative contribution of the reionization contribution to the S/N decreases, while the relative contribution of the multipoles around $\ell \approx 90$ (where the B -mode spectrum is expected to have a maximum) increases (see Fig. 3). Thus, the contribution of RGWs at higher multipoles ($\ell \sim 100$) becomes significant, which in turn increases the value of the best-pivot multipole. Second, when \hat{r}^* is large, the contributions from the C , T , E power spectra become important in constraining r and n_t [40]. For these power spectra, the main contribution to the signal comes from the multipoles $10 \lesssim \ell \lesssim 100$ [40]. This again leads to an increase in the value of ℓ_t^* .

The middle panel in Fig. 2 shows the signal-to-noise ratio S/N as a function of \hat{r}^* . As expected, the signal-to-noise ratio rises with the increase of \hat{r}^* . Setting the threshold value of $S/N = 2$, we can determine the detection possibilities for the three considered examples: $\hat{r}^* \geq 0.05$ for Planck noises; $\hat{r}^* \geq 1.5 \times 10^{-4}$ for the case with cosmic lensing; $\hat{r}^* \geq 3.7 \times 10^{-6}$ for the case with the reduced cosmic lensing. These estimations are consistent with previous results [22,41–43].

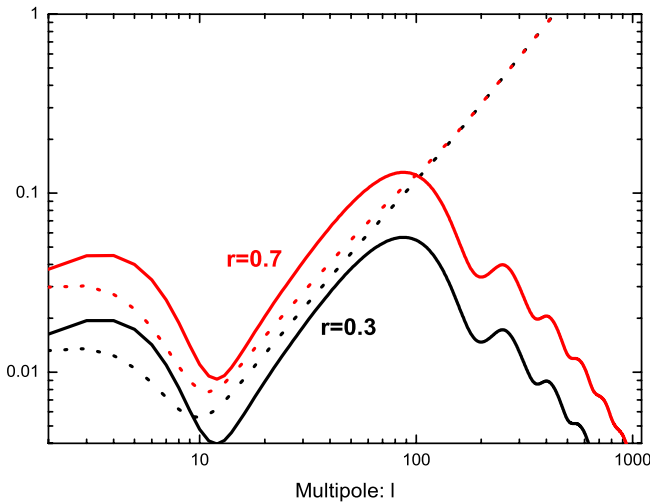


FIG. 3 (color online). The comparison of \hat{C}_ℓ^B and $\hat{\sigma}_{D_\ell^B}$ [which enter the expression for signal-to-noise ratio S/N (53)], for models with $\hat{r}^* = 0.3$ (black lines) and $\hat{r}^* = 0.7$ (red lines). The solid lines show the “signal” term (i.e. power spectrum) $\ell(\ell+1)\hat{C}_\ell^B/2\pi$ (μK^2), and dotted lines show the “noise” term $\ell(\ell+1)\hat{\sigma}_{D_\ell^B}/2\pi$ (μK^2). The quantity $\hat{\sigma}_{D_\ell^B}$ was calculated using the Planck noises (15).

Finally, the right panel in Fig. 2 presents the achievable constraints on the spectral index Δn_t as a function of \hat{r}^* . As expected, the uncertainty in determining the spectral index drops with the increase of the input value \hat{r}^* . For the case of the Planck mission, the uncertainty in estimation of n_t always remains fairly large. Even for large value $\hat{r}^* = 1$ the constraint on the spectral index is $\Delta n_t = 0.08$ (for comparison, the Planck mission will be able to achieve a constraint of $\Delta n_s = 0.0045$ on the spectral index of density perturbations [1]). For a value $\hat{r}^* = 0.1$, the constraint on the spectral index is $\Delta n_t = 0.25$, which is too large to constrain inflationary models or to verify the consistency relation. Potentially, in an idealized situation with reduced cosmic lensing, for $\hat{r}^* = 0.1$, we can constrain the spectral index to the level $\Delta n_t = 0.007$. If this accuracy can be achieved in the future, it will place a fairly tight constraint on inflationary models.

IV. COMPARISON WITH NUMERICAL SIMULATIONS

In Sec. III we have analytically studied the likelihood analysis of the RGW parameters r^* , n_t and r , as well as introduced the best-pivot multipole ℓ_t^* (corresponding to the best-pivot wave number k_t^*) and explained its significance. We have analytically derived expressions for the uncertainties of the RGW parameters and the value of the best-pivot multipole, in terms of the CMB power spectra, experimental uncertainties and the estimators of the CMB power spectra. In this section we shall compare the analytical results of the previous section with numerical simulations. We shall show that, although we have used a number of approximations, the analytical results are in good agreement with the exact numerical results based on the analysis of simulated data.

This section is separated into two parts. In the first subsection, using a single simulated data set $\{D_\ell^X\}$, we shall use the MCMC techniques to construct the posterior pdf for the RGW parameters. We shall calculate the uncertainties and correlations associated with the parameters, and compare these values with the analytical predictions in Secs. III C and III D. In the second subsection we shall generate 300 samples of data sets $\{D_\ell^X\}$. For each individual sample, using the posterior pdf $P(r^*, n_t)$ we shall calculate the estimates for the RGW parameters r_{ML}^* , $n_{t\text{ML}}^*$ and r_{ML} . Analyzing the distribution of these estimates, we shall evaluate the mean values and the standard deviation, and compare these with the analytical predictions from Sec. III E.

A. Likelihood analysis of a single simulated data set

In this subsection, from a single simulated data set $\{D_\ell^X\}$, using the likelihood analysis procedure, we shall derive the constraints on the tensor-to-scalar ratio and the RGW primordial spectral index.

In order to simulate the CMB data, we shall randomly draw a data set $\{D_\ell^X\}$, from an underlying pdf (A1) (see the appendix). This pdf depends on the input cosmological model and characteristics of the CMB experiment. We shall choose as an input cosmological model a model with the background cosmological parameters given in (8) and the contribution of density perturbation (9). The input parameters for the RGW field will be chosen as

$$\hat{r} = 0.3, \quad \hat{n}_t = 0.0. \quad (55)$$

To characterize the properties of the CMB experiment, namely, the power spectra of noises, the cut sky factor and the window function, we shall adopt the values specified for the Planck satellite mission (15) [1].

In order to simulate and analyze the data, we proceed as follows:

- (1) We generate a single data sample $\{D_\ell^Y|Y = C, T, E, B; \ell = 2, 3, \dots, 1000\}$, drawn from the pdf (A1).
- (2) Using (30), we calculate the best-pivot multipole scale $\ell_t^* = 21.1$ (corresponding to the best-pivot wave number $k_t^* = 0.002 \text{ Mpc}^{-1}$). Note that the value of ℓ_t^* does not depend on the concrete realization generated in step 1.
- (3) Using the MCMC method (see [45] for details), we construct the likelihood function \mathcal{L} as a function of two free parameters r^* and n_t , with the other cosmological parameters fixed at their ‘‘best-fit’’ values given by (8) and (9). Choosing a uniform prior we build the posterior pdf $P(r^*, n_t)$ (which is exactly equal to the likelihood function \mathcal{L} [see (24) and (25)]).
- (4) Using the posterior pdf $P(r^*, n_t)$, we find the maximum-likelihood values $(r_{\text{ML}}^*, n_{\text{ML}})$, and plot the contours corresponding to 68.3% and 95.4% confidence interval regions in the (r^*, n_t) plane surrounding these values. We also calculate the one-dimensional posterior pdfs for variables r^* and n_t . From $P(r^*, n_t)$, we calculate the uncertainties Δr^* and Δn_t . Using the importance sample technique (see [45,46]), we evaluate the correlation coefficient $\rho_{(r^*, n_t)}$ defined in (42).
- (5) We now choose a different value of the pivot wave number $k_0 = 0.05 \text{ Mpc}^{-1}$, corresponding to the value for the pivot multipole $\ell_0 = 500$. Using (43), we calculate the tensor-to-scalar ratio for this pivot wave number r as a function of the parameters r^* and n_t . From the posterior probability function $P(r^*, n_t)$, using the importance sample technique, we can obtain the uncertainty $\Delta \ln r$ and the correlation coefficient $\rho_{(n_t, \ln r)}$ defined in (46).

The results of the simulation and analysis are shown in Fig. 4. The panels on the top show the constraints in the $r^* - n_t$ plane (top-left), and the one-dimensional posterior pdfs for r^* (top-middle) and n_t (top-right). The constraint on the parameters r^* and n_t , together with the correlation

coefficient are as follows:

$$\begin{aligned} r^* &= 0.343_{-0.053}^{+0.047} \quad (68.3\% \text{C.L.}); \\ n_t &= -0.067_{-0.130}^{+0.146} \quad (68.3\% \text{C.L.}); \\ \rho_{(r^*, n_t)} &= -0.02 \quad (\text{simulation results}). \end{aligned} \quad (56)$$

For comparison, the analytical formulas (40)–(42) yield the following results for these quantities:

$$\begin{aligned} r_{\text{ML}}^* \pm \Delta r^* &= 0.345 \pm 0.047; \\ n_{\text{ML}} \pm \Delta n_t &= -0.062 \pm 0.135; \\ \rho_{(r^*, n_t)} &= 0 \quad (\text{analytical results}). \end{aligned} \quad (57)$$

As can be seen, the analytical results (57) are in good agreement with results of simulation (56).

The bottom panels in Fig. 4 show the constraints in the $\ln r - n_t$ plane (bottom-left), and the one-dimensional posterior pdfs for $\ln r$ (bottom-middle). As expected, the confidence interval contours in the $\ln r - n_t$ indicate a strong correlation between $\ln r$ and n_t . The corresponding constraints and correlation coefficient are as follows:

$$\begin{aligned} \ln r &= -1.299_{-0.413}^{+0.527} \quad (68.3\% \text{C.L.}); \\ \rho_{(n_t, \ln r)} &= 0.95 \quad (\text{simulation results}). \end{aligned} \quad (58)$$

The analytical expressions (44), (45), and (47) yield the following results for these quantities:

$$\begin{aligned} \ln r_{\text{ML}} \pm \Delta \ln r &= -1.307 \pm 0.456; \\ \rho_{(n_t, \ln r)} &= 0.94 \quad (\text{analytical results}). \end{aligned} \quad (59)$$

Once again, we find that analytical and the exact results are consistent with each other.

Furthermore, we have applied the same simulation and analysis procedure to the case with the ‘‘cosmic lensing’’ noises [see (16)], for input values of tensor-to-scalar ratio $\hat{r}^* = 0.1, 0.2$ and 0.3 . We found that in all these cases, the numerical estimations for Δr^* , $\Delta \ln r$ and Δn_t agree with the analytical expression to within 20%. Thus the analytical formulas for Δr^* , $\Delta \ln r$ and Δn_t seem to be accurate.

B. Maximum-likelihood analysis in numerical data simulations

In this subsection, we shall discuss the distribution of the maximum-likelihood estimators for the RGW parameters r_{ML}^* , r_{ML} and n_{ML} in multiple realizations. We shall generate a simulated CMB data set $\{D_\ell^X\}$ a number of times. For each individual realization we shall calculate the estimators r_{ML}^* , r_{ML} and n_{ML} . We shall then analyze the distribution of these parameters and compare these results with analytical calculations.

In order to generate and analyze the data, we proceed in the following manner:

- (1) A collection of 300 samples of data sets $\{D_\ell^Y|Y = T, E, B, C; \ell = 2, 3, \dots, 1000\}$ is randomly gener-

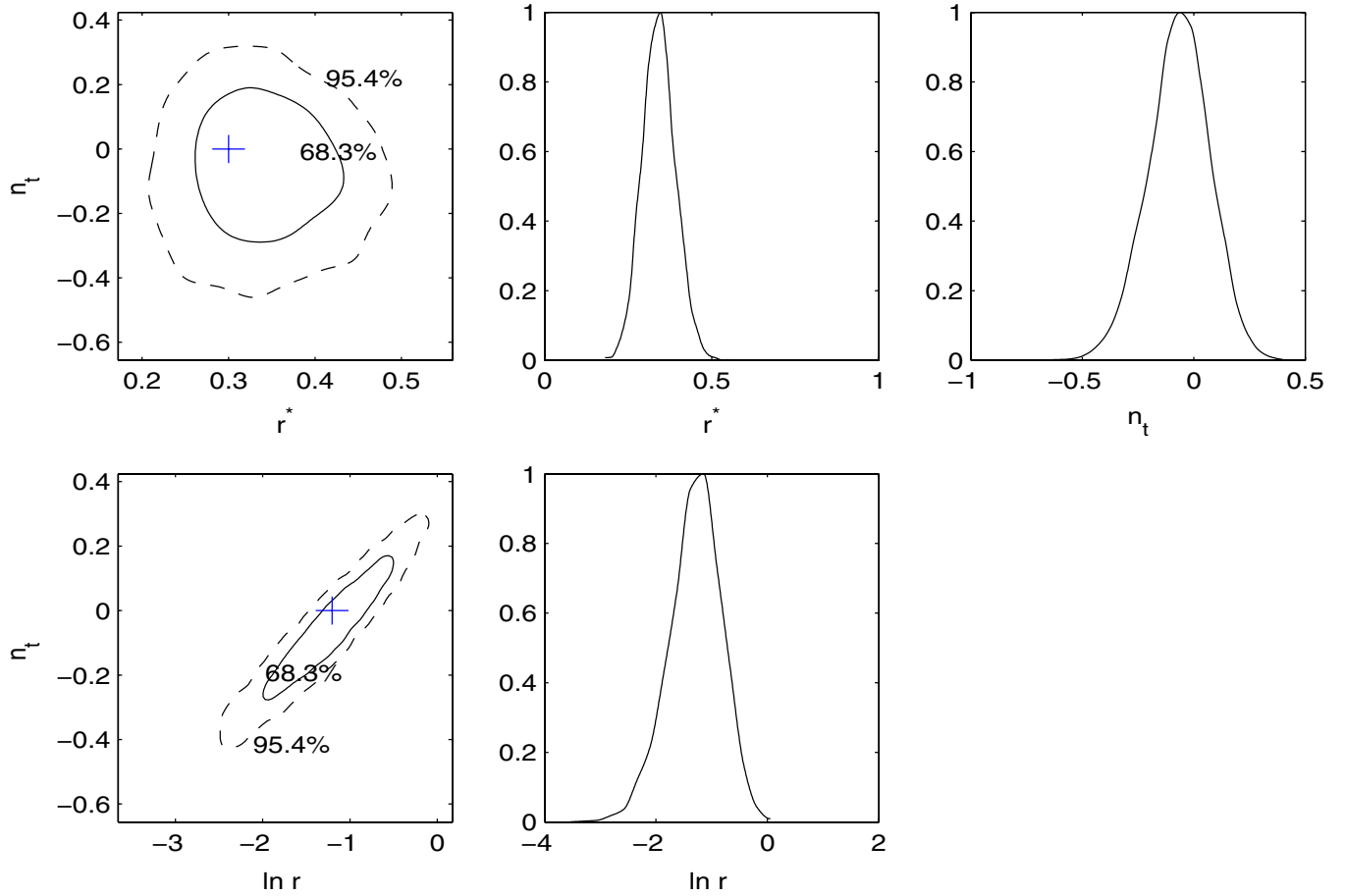


FIG. 4 (color online). Two-dimensional and one-dimensional posterior constraints for parameters: r^* and n_t (upper panels), and for parameters: $\ln r$ and n_t (lower panels). The blue + in the left panels indicates the value of the input model parameters.

ated from an underlying pdf $f(D_\ell^C, D_\ell^T, D_\ell^E, D_\ell^B)$, given in (A1). The input cosmological model and the noise characteristics of the CMB experiment are chosen in the same manner as in Sec. IVA.

- (2) Using (30), we calculate the best-pivot multipole $\ell_t^* = 21.1$ (corresponding to the best-pivot wave number $k_t^* = 0.002 \text{ Mpc}^{-1}$). Note that the value of ℓ_t^* does not depend on the concrete realization generated in step 1.
- (3) For each individual sample, we construct the likelihood function \mathcal{L} as a function of variables r^* and n_t , which is equal to the posterior pdf $P(r^*, n_t)$ [see (24) and (25)]. For each individual sample, an automated search (which uses the numerical technique of the simulated annealing [47]) determines the maximum-likelihood estimators r_{ML}^* and $n_{t\text{ML}}$ [at which the posterior pdf $P(r^*, n_t)$ reaches a maximum]. The calculated values r_{ML}^* and $n_{t\text{ML}}$ are plotted in Fig. 5 (left panel).
- (4) We adopt a different pivot wave number $k_0 = 0.05 \text{ Mpc}^{-1}$, corresponding to the value for the pivot multipole $\ell_0 = 500$. From the set of values $(r_{\text{ML}}^*, n_{t\text{ML}})$, we calculate the corresponding values

of tensor-to-scalar ratio for the new pivot wave number r_{ML} using (43). The resulting values are illustrated in Fig. 5 (right panel).

The mean values and standard deviations for the quantities r_{ML}^* and $n_{t\text{ML}}$ [shown in Fig. 5 (left panel)], obtained from the analysis of the simulated data, are

$$\begin{aligned} \langle r_{\text{ML}}^* \rangle \pm \sigma_{r_{\text{ML}}^*} &= 0.298 \pm 0.046; \\ \langle n_{t\text{ML}} \rangle \pm \sigma_{n_{t\text{ML}}} &= -0.001 \pm 0.152 \quad (\text{simulation results}). \end{aligned} \quad (60)$$

For comparison, we can calculate the corresponding quantities using the analytical expressions derived in Sec. III. Using (50) and (51), we obtain

$$\begin{aligned} \langle r_{\text{ML}}^* \rangle \pm \sigma_{r_{\text{ML}}^*} &= 0.300 \pm 0.047; \\ \langle n_{t\text{ML}} \rangle \pm \sigma_{n_{t\text{ML}}} &= 0 \pm 0.135 \quad (\text{analytical results}). \end{aligned} \quad (61)$$

Comparing (61) with (60), we find that the analytical expressions are in good agreement with results of numerical simulation.

In a similar fashion, for the mean values and the standard deviation of quantity r_{ML} [shown in Fig. 5 (right panel)], we obtain

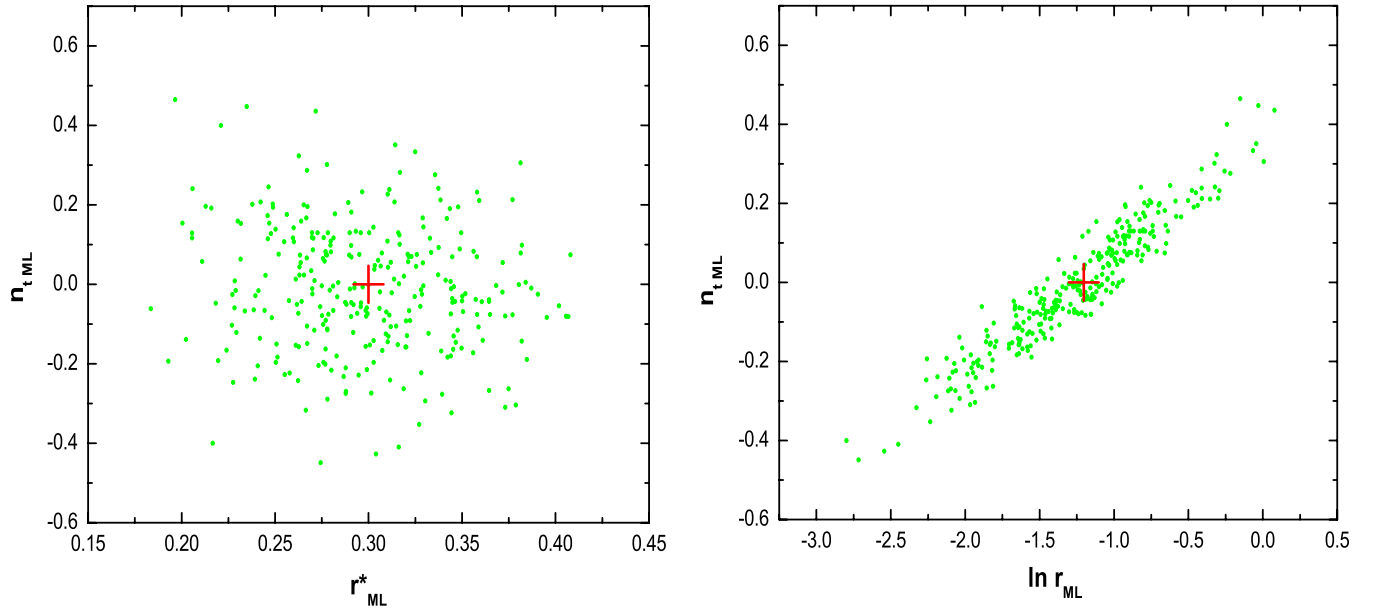


FIG. 5 (color online). The values of the ML estimators from 300 simulations are shown projected onto the $n_{t,ML} - r_{ML}^*$ plane (left panel), and $n_{t,ML} - \ln r_{ML}$ plane (right panel). The red + indicates the value of the input model parameters.

$$\langle \ln r_{ML} \rangle \pm \sigma_{\ln r_{ML}} = -1.252 \pm 0.508 \quad (\text{simulation result}). \quad (62)$$

The analytical expressions (50) and (51) yield the following results:

$$\langle \ln r_{ML} \rangle \pm \sigma_{\ln r_{ML}} = -1.204 \pm 0.456 \quad (\text{analytical result}). \quad (63)$$

Comparing (62) with (63), we find a reasonable agreement to within 10%.

V. CONCLUSION

In this paper, we have analyzed the potential joint constraints on the two parameters characterizing the RGW background, the tensor-to-scalar ratio r and the tensor primordial spectral index n_t , achievable by the upcoming CMB observations. We have shown that, in general, there exists a correlation between the parameters r and n_t . However, when considering the tensor-to-scalar ratio r^* defined at the best-pivot multipole number ℓ_t^* , the correlation between r^* and n_t disappears. Furthermore, the uncertainty Δr^* has the least possible value. We have derived analytical formulas for calculating ℓ_t^* , Δr^* , Δn_t , Δr , and the correlation coefficient between r and n_t . Using numerical simulations of future CMB data we have verified the robustness of our analytical estimations and have shown that our fairly simple analytical expressions agree with exact numerical evaluations to within 20%. We have also discussed the dependence of our results on the background cosmological model, the amplitude of the RGWs, and the characteristics of the CMB experiment. We have studied the dependence of the signal-to-noise ratio S/N along with

the value of the best-pivot multipole ℓ_t^* and the uncertainty Δn_t on the amplitude of the RGWs. We show that, although the Planck satellite will potentially be able to measure the tensor-to-scalar ratio to a level $r \gtrsim 0.05$ (at 2σ C.L.), the uncertainty in determining the spectral index will remain fairly large $\Delta n_t \gtrsim 0.25$ (for $r = 0.1$). Thus, for example, the Planck satellite will not be able to verify the so-called consistency relation $n_t = -r/8$. In an idealized scenario, where the noises are limited by reduced cosmic lensing noise, the precision $\Delta n_t \gtrsim 0.007$ (for $r = 0.1$) is achievable, thus potentially allowing tight constraints on possible inflationary scenarios. The analytical results presented here provide a simple and quick method to investigate the ability of the future CMB observations to detect RGWs.

ACKNOWLEDGMENTS

The authors thank L.P. Grishchuk for helpful discussions and useful suggestions. W.Z. is partly supported by Chinese NSF under Grants No. 10703005 and No. 10775119. In this paper, we have used the CAMB code for calculating the various CMB power spectra [37].

APPENDIX: EXACT PROBABILITY DENSITY FUNCTIONS FOR D_ℓ^Y AND LIKELIHOOD FUNCTION

In [22] (see also [40,48,49]) we have derived the pdfs for the best unbiased estimators D_ℓ^Y of the various CMB power spectra C_ℓ^Y . These were derived under the assumption that the primordial perturbations (density perturbations and RGWs) are isotropic and homogeneous Gaussian random

fields, and that the noises associated with the CMB measurements can be assumed Gaussian. In this appendix we shall briefly list the main results that have been used in the present paper.

The joint pdf for the estimators D_ℓ^T , D_ℓ^E , D_ℓ^B and D_ℓ^C has the following form:

$$f(D_\ell^C, D_\ell^T, D_\ell^E, D_\ell^B) = f(D_\ell^C, D_\ell^T, D_\ell^E) f(D_\ell^B), \quad (\text{A1})$$

where the pdf $f(D_\ell^B)$ has the form of the χ^2 distribution

$$f(D_\ell^B) = \frac{(n_e W_\ell^2)^{n_e} e^{-v/2}}{2^{n_e/2} \Gamma(n_e/2) (\sigma_\ell^B)^2}, \quad (\text{A2})$$

and the joint pdf $f(D_\ell^C, D_\ell^T, D_\ell^E)$ is the Wishart distribution

$$\begin{aligned} f(D_\ell^C, D_\ell^T, D_\ell^E) &= \left\{ \frac{1}{4(1-\rho_\ell^2)(\sigma_\ell^T \sigma_\ell^E)^2} \right\}^{n_e/2} \\ &\times \frac{(n_e W_\ell^2)^3 (xy - z^2)^{(n_e-3)/2}}{\pi^{1/2} \Gamma(n_e/2) \Gamma((n_e-1)/2)} \\ &\times \exp \left\{ -\frac{1}{2(1-\rho_\ell^2)} \left(\frac{x}{(\sigma_\ell^T)^2} + \frac{y}{(\sigma_\ell^E)^2} \right. \right. \\ &\left. \left. - \frac{2\rho_\ell z}{\sigma_\ell^T \sigma_\ell^E} \right) \right\}. \quad (\text{A3}) \end{aligned}$$

In the above expressions (A2) and (A3), C_ℓ^Y are the corresponding CMB power spectra, N_ℓ^Y are the noise power spectra, and W_ℓ is the window function. The quantity $n_e = (2\ell + 1)f_{\text{sky}}$ is the effective degree of freedom for a particular multipole ℓ in the case of partial sky coverage with

the cut sky factor f_{sky} . The quantities v , x , y , and z are defined as follows:

$$\begin{aligned} v &\equiv n_e (D_\ell^B W_\ell^2 + N_\ell^B) / (C_\ell^B W_\ell^2 + N_\ell^B), \\ x &\equiv n_e (D_\ell^T W_\ell^2 + N_\ell^T), \\ y &\equiv n_e (D_\ell^E W_\ell^2 + N_\ell^E), \\ z &\equiv n_e D_\ell^C W_\ell^2. \end{aligned}$$

In (A2), σ_ℓ^B is the standard deviation for the multipole coefficient $a_{\ell m}^B$. The quantities σ_ℓ^T , σ_ℓ^E and ρ_ℓ in (A3) are correspondingly the standard deviations and the correlation coefficient for the multipole coefficients $a_{\ell m}^T$ and $a_{\ell m}^E$. These are expressible in terms of the CMB and noise power spectra in the following form:

$$\begin{aligned} \sigma_\ell^T &= \sqrt{C_\ell^T W_\ell^2 + N_\ell^T}, \\ \sigma_\ell^E &= \sqrt{C_\ell^E W_\ell^2 + N_\ell^E}, \\ \sigma_\ell^B &= \sqrt{C_\ell^B W_\ell^2 + N_\ell^B}, \\ \rho_\ell &= C_\ell^C / \sqrt{(C_\ell^T + N_\ell^T W_\ell^{-2})(C_\ell^E + N_\ell^E W_\ell^{-2})}. \end{aligned}$$

Finally, the likelihood function \mathcal{L} introduced in Sec. III A is, up to a constant of normalization, the product of the joint pdf $f(D_\ell^C, D_\ell^T, D_\ell^E, D_\ell^B)$, i.e.

$$\mathcal{L} \propto \prod_\ell f(D_\ell^C, D_\ell^T, D_\ell^E, D_\ell^B). \quad (\text{A4})$$

-
- [1] Planck Collaboration, arXiv:astro-ph/0604069.
[2] M. R. Nolte *et al.*, *Astrophys. J. Suppl. Ser.* **180**, 296 (2009).
[3] B. G. Keating *et al.*, in *Polarimetry in Astronomy*, edited by Silvano Fineschi, Proc. SPIE Int. Soc. Opt. Eng. Vol. 4843 (SPIE-International Society for Optical Engineering, Bellingham, WA, 2003); C. Pryke *et al.* (QUaD Collaboration), *Astrophys. J.* **692**, 1247 (2009); A. C. Taylor *et al.* (Clover Collaboration), *New Astron. Rev.* **50**, 993 (2006); C. Bischoff *et al.* (CAPMAP Collaboration), *Astrophys. J.* **684**, 771 (2008); D. Samtleben, arXiv:0806.4334.
[4] P. Oxley *et al.*, Proc. SPIE Int. Soc. Opt. Eng. **5543**, 320 (2004); B. P. Crill *et al.*, arXiv:0807.1548.
[5] D. Baumann *et al.*, arXiv:0811.3919.
[6] L. P. Grishchuk, *Zh. Eksp. Teor. Fiz.* **67**, 825 (1974) [*Sov. Phys. JETP* **40**, 409 (1975)]; *Ann. N.Y. Acad. Sci.* **302**, 439 (1977); *Pis'ma Zh. Eksp. Teor. Fiz.* **23**, 326 (1976) [*JETP Lett.* **23**, 293 (1976)].
[7] L. P. Grishchuk, V. M. Lipunov, K. A. Postnov, M. E. Prokhorov, and B. S. Sathyaprakash, *Phys. Usp.* **44**, 1 (2001); M. Maggiore, *Phys. Rep.* **331**, 283 (2000).
[8] A. A. Starobinsky, *JETP Lett.* **30**, 682 (1979).
[9] V. A. Rubakov, M. Sazhin, and A. Veryaskin, *Phys. Lett.* **115B**, 189 (1982).
[10] S. Sasaki, *Prog. Theor. Phys.* **76**, 1036 (1986).
[11] V. F. Mukhanov, H. A. Feldman, and R. H. Brandenberger, *Phys. Rep.* **215**, 203 (1992).
[12] L. P. Grishchuk, *Lect. Notes Phys.* **562**, 167 (2001); Y. Zhang, Y. F. Yuan, W. Zhao, and Y. T. Chen, *Classical Quantum Gravity* **22**, 1383 (2005); T. L. Smith, H. V. Peiris, and A. Cooray, *Phys. Rev. D* **73**, 123503 (2006); W. Zhao and Y. Zhang, *Phys. Rev. D* **74**, 043503 (2006).
[13] Y. Watanabe and E. Komatsu, *Phys. Rev. D* **73**, 123515 (2006); L. A. Boyle and P. J. Steinhardt, *Phys. Rev. D* **77**, 063504 (2008); M. Giovannini, *Phys. Rev. D* **60**, 123511 (1999); *Classical Quantum Gravity* **16**, 2905 (1999); *Phys. Lett. B* **668**, 44 (2008).
[14] A. Polnarev, *Sov. Astron.* **29**, 607 (1985); D. Harari and M. Zaldarriaga, *Phys. Lett. B* **319**, 96 (1993); L. P. Grishchuk, *Phys. Rev. Lett.* **70**, 2371 (1993); R. Crittenden, J. R. Bond, R. L. Davis, G. Efstathiou, and P. J. Steinhardt, *Phys. Rev. Lett.* **71**, 324 (1993); R. A. Frewin, A. G. Polnarev, and P. Coles, *Mon. Not. R. Astron. Soc.* **266**,

- L21 (1994).
- [15] U. Seljak and M. Zaldarriaga, Phys. Rev. Lett. **78**, 2054 (1997); M. Kamionkowski, A. Kosowsky, and A. Stebbins, Phys. Rev. D **55**, 7368 (1997).
- [16] M. Zaldarriaga and U. Seljak, Phys. Rev. D **55**, 1830 (1997).
- [17] J.R. Pritchard and M. Kamionkowski, Ann. Phys. (N.Y.) **318**, 2 (2005); W. Zhao and Y. Zhang, Phys. Rev. D **74**, 083006 (2006); T. Y. Xia and Y. Zhang, Phys. Rev. D **78**, 123005 (2008).
- [18] D. Baskaran, L.P. Grishchuk, and A.G. Polnarev, Phys. Rev. D **74**, 083008 (2006).
- [19] B.G. Keating, A.G. Polnarev, N.J. Miller, and D. Baskaran, Int. J. Mod. Phys. A **21**, 2459 (2006); R. Flauger and S. Weinberg, Phys. Rev. D **75**, 123505 (2007); Y. Zhang, W. Zhao, X.Z. Er, H.X. Miao, and T. Y. Xia, Int. J. Mod. Phys. D **17**, 1105 (2008).
- [20] L.P. Grishchuk, arXiv:0707.3319.
- [21] A.G. Polnarev, N.J. Miller, and B.G. Keating, Mon. Not. R. Astron. Soc. **386**, 1053 (2008); N.J. Miller and B.G. Keating, and A.G. Polnarev, arXiv:0710.3651.
- [22] W. Zhao, D. Baskaran, and L.P. Grishchuk, Phys. Rev. D **79**, 023002 (2009).
- [23] R.G. Crittenden, D. Coulson, and N.G. Turok, Phys. Rev. D **52**, R5402 (1995).
- [24] A. Melchiorri and C.J. Odman, Phys. Rev. D **67**, 021501(R) (2003).
- [25] E. Komastu *et al.*, Astrophys. J. Suppl. Ser. **180**, 330 (2009); A. Lewis, Phys. Rev. D **78**, 023002 (2008); J.Q. Xia, H. Li, G. B. Zhao, and X. M. Zhang, Phys. Rev. D **78**, 083524 (2008); L.P.L. Colombo, E. Pierpaoli, and J.R. Pritchard, arXiv:0811.2622.
- [26] E.D. Stewart and D.H. Lyth, Phys. Lett. B **302**, 171 (1993).
- [27] D.H. Lyth and A. Riotto, Phys. Rep. **314**, 1 (1999).
- [28] D. Polarski and A. A. Starobinsky, Phys. Lett. B **356**, 196 (1995).
- [29] L.P. Grishchuk, Usp. Fiz. Nauk **175**, 1289 (2005) [Phys. Usp. **48**, 1235 (2005)].
- [30] L.P. Grishchuk and M. Solokhin, Phys. Rev. D **43**, 2566 (1991).
- [31] R.H. Brandenberger, A. Nayeri, S.P. Patil, and C. Vafa, Phys. Rev. Lett. **98**, 231302 (2007).
- [32] J. Grain and A. Barrau, Phys. Rev. Lett. **102**, 081301 (2009).
- [33] L.P.L. Colombo, E. Pierpaoli, and J.R. Pritchard, arXiv:0811.2622.
- [34] L. Knox, Phys. Rev. D **52**, 4307 (1995).
- [35] <http://cosmologist.info/notes/CAMB.pdf>.
- [36] H.V. Peiris *et al.*, Astrophys. J. Suppl. Ser. **148**, 213 (2003).
- [37] <http://camb.info/>.
- [38] D.N. Spergel *et al.*, Astrophys. J. Suppl. Ser. **170**, 377 (2007).
- [39] A. Kosowsky, M. Milosavljevic, and R. Jimenez, Phys. Rev. D **66**, 063007 (2002).
- [40] W. Zhao, Phys. Rev. D **79**, 063003 (2009).
- [41] W. Hu and T. Okamoto, Astrophys. J. **574**, 566 (2002); T. Okamoto and W. Hu, Phys. Rev. D **67**, 083002 (2003); M. Kesden, A. Cooray, and M. Kamionkowski, Phys. Rev. Lett. **89**, 011304 (2002); L. Knox and Y.S. Song, Phys. Rev. Lett. **89**, 011303 (2002).
- [42] A. Lewis and A. Challinor, Phys. Rep. **429**, 1 (2006).
- [43] C.M. Hirata and U. Seljak, Phys. Rev. D **68**, 083002 (2003); U. Seljak and C.M. Hirata, Phys. Rev. D **69**, 043005 (2004).
- [44] J. Dunkley *et al.*, arXiv:0811.3915; A.A. Fraise *et al.*, arXiv:0811.3920.
- [45] A. Lewis and S.L. Bridle, Phys. Rev. D **66**, 103511 (2002).
- [46] A. Gelman, J.B. Carlin, H.S. Stern, and D.B. Rubin, *Bayesian Data Analysis* (ACRC Press, Boca Raton, FL, 2004); W.R. Gilks, S. Richardson, and D.J. Spiegelhalter, *Markov Chain Monte Carlo in Practice* (ACRC Press, Boca Raton, FL, 1996).
- [47] W.H. Press, B.P. Flannery, S.A. Teukolsky, and W.T. Vetterling, *Numerical Recipes (FORTRAN)* (Cambridge University Press, Cambridge, England, 1989).
- [48] S. Hamimeche and A. Lewis, Phys. Rev. D **77**, 103013 (2008).
- [49] W.J. Percival and M.L. Brown, Mon. Not. R. Astron. Soc. **372**, 1104 (2006); H.K. Eriksen and I.K. Wehus, Astrophys. J. Suppl. Ser. **180**, 30 (2009).